RSC Advances

PAPER

View Article Online
View Journal | View Issue

Cite this: *RSC Adv.*, 2025, **15**, 24739

Molecular imprinted polymer-based metal complex potentiometric sensor doped with carbon nanotubes for sensitive determination of piroxicam in spiked human plasma†

Veronia S. Nazim, Ghada M. El-Sayed, Sawsan M. Amer and Ahmed H. Nadim*

The main concern upon fabrication of solid contact potentiometric electrodes is the choice of ion sensing membrane. The key principle is to design a sensor having optimum sensitivity and potential stability along with simplicity, reproducibility, and cost effectiveness. Herein, a novel screen-printed potentiometric sensor has been developed for selective and sensitive determination of piroxicam in its pharmaceutical formulation or human plasma. The obstacle was to improve the limit of detection of the proposed sensor to determine the plasma peak concentration of the cited drug. A three-step optimization protocol has been developed. (I) Novel neutral carrier based on Cu(II) complex of piroxicam was employed as ion sensing membrane with better sensitivity compared to classical ion exchangers. (II) The sensor was fabricated based on molecular imprinted polymer of piroxicam to assure selectivity. Molecular imprinted polymer was synthesized by precipitation polymerization approach and characterized by field-emission scanning electron microscope, Fourier-transform infrared spectroscopy, and Brunauer–Emmett–Teller measurements for surface area analysis. (III) The obstacle of water layer formation was overcomed by comparing the doping effect of multiwalled carbon nanotubes and graphene nanocomposite on the sensors' signal stability. Three screen printed sensors for piroxicam were developed and their electrochemical performance was assessed. Optimum results for piroxicam were obtained with ion sensing membrane of Cu(II)-piroxicam complex based on molecular imprinting and multiwalled carbon nanotubes. The obtained Nernstian slope was 28.97 mV/decade with linearity range of 9.7×10^{-7}–1×10^{-3} M and LOD of 5.2×10^{-7} M. The sensor was successfully applied into spiked human plasma. This would offer an alternative sensing platform for therapeutic monitoring of piroxicam in biological fluids.

Received 31st May 2025
Accepted 7th July 2025

DOI: 10.1039/d5ra03851k

rsc.li/rsc-advances

1 Introduction

Electrochemical methods have recently experienced a massive increase in applications owing to the sensitivity and selectivity of their measurements.[1] Potentiometric ion selective electrodes (ISE) offer several advantages compared to other electrochemical methods, including short response time, high lifetime, low cost, and wide detection ranges for different analyte determination.[2–4] Solid contact ion-selective electrodes (SC-ISE) are advanced potentiometric sensors with the capability of detection of a wide range of analytes in industrial processes as well as clinical analysis.[5] Recently, the innovative design of SC-ISE offers great advantages to improve potential stability and miniaturization for *in situ*/real-time analysis.[6] Ion sensing membrane (ISM), an integral part of ISE, can selectively detect the concentration of a specific ion with respect to the reference electrode. Polymer-based ISMs have been widely used regardless the specific requirements of individual application.[7] There is an urgent need for sensitive and selective determination of traces of specific anionic species in a wide variety of real samples. Ion sensing membranes based on metal centers as binding sites are often applied for anionic sensors. The metal center can be either ionic, complexed in an organic ligand, or can be covalently bound as part of an organometallic structure. The ligands surrounding the metal center in a complex can be modified to suit specific analytes. By adjusting the ligand structure, the complex can be made to preferentially bind certain ions or molecules, offering a high degree of selectivity. This tunability makes metal complexes ideal for the design of specific ion-selective electrodes tailored to particular ions even in complex matrices.[8,9] A recent study reported Bakker *et al.* showed the behavior of calcium ion complexation and utilizing an isomeric calcium complex as ionophore for selective determination of ionized calcium in blood samples[10] with promising outcomes.

Pharmaceutical Analytical Chemistry Department, Faculty of Pharmacy, Cairo University, Egypt. E-mail: ahmed.nagib@pharma.cu.edu.eg

† Electronic supplementary information (ESI) available. See DOI: https://doi.org/10.1039/d5ra03851k

A globally widespread used class of drugs is the non-steroidal anti-inflammatory drugs (NSAIDs), particularly aspirin, ibuprofen, diclofenac, meloxicam, and piroxicam. The frequent consumption of these drugs is due to their characteristic properties; anti-inflammatory, analgesic, and antipyretic actions.[11] Among NSAIDs class, piroxicam (PXM) (4-hydroxy-2-methyl-N-2 pyridinyl-2*H*-1,2-benzothiazino-3-carboxamide-1,1-dioxide) is an enolic acid oxicam derivative. It is commonly prescribed for therapeutic treatment of rheumatoid arthritis, osteoarthritis, and spondylitis, thus it is usually prescribed for chronic conditions.[12] The association between cardiovascular complications and the use of NSAIDs is an area of ongoing concern. NSAIDs may increase the risk of serious adverse cardiovascular thrombotic events.[13] PXM inhibits platelet aggregation and may prolong bleeding time. Some reports have also suggested that the incidence of piroxicam-induced peptic ulceration and gastrointestinal bleeding may be higher with usual dosages compared to other NSAIDs.[14] To minimize the potential adverse effects, the lowest effective dosage and shortest possible duration of therapy should be employed and monitored regularly.

Different methods for analysis are reported in the literature for detection of PXM in various samples such as liquid chromatographic,[15–18] spectrophotometric[19–21] and electrochemical methods.[22–25] Nevertheless, most of these reported methods require expensive instrumentation and involve several manipulation steps and sample pre-treatment before analysis. The development of a simple, rapid and cost-effective approach with a low detection limit for PXM determination is of great interest. Screen printed sensors have the advantages of simplicity, short analysis time with adequate precision and accuracy.[26] Moreover, they are highly suitable for portable instrumentation and offer several advantages being simple to prepare, highly sensitive and cost effective.[27] A key feature of these sensors is their disposability, which ensures sensitivity as they are designed for single use only which presents a significant advantage over conventional sensors for real-time and *in situ* monitoring of biological samples.[28] The sensor's detection limit should be lower than the concentration range in physiological condition to reach optimal performance. This enhances the sensor's ability to monitor and assess target concentrations effectively, leading to better diagnostic and monitoring capabilities. The choice of ion sensing membrane for fabrication of electrochemical sensors is a main concern. Several potentiometric methods were reported for PXM determination using the classical anion exchangers as a sensing platform with acceptable detection limit.[22,29–32] The design of metal carriers such as some aza-substituted macrocyclic ligands, metallocenes, porphyrins, phthalocyanines and Schiff base metal complexes as sensing membranes have emerged to obtain more sensitive, selective and cost effective for determination of analytes.[33,34] PXM was found to be highly selective to complexation with Cu(II) ions.[35] Therefore, a Cu(II) PXM complex was prepared and employed as a sensing platform in ISE. Moreover, the electrode selectivity can be tuned by adding either a traditional ionophore[36] or a specifically synthesized molecular imprinted polymer (MIP)[37] for the cited drug. MIP are three-dimensional polymeric materials with cavities complementary to the template drug. These cavities act as receptors that can bind specifically to the drug of interest.[38] Another approach to enhance the sensors' performance was employing nanoparticles in fabrication and optimization of electrodes.[39] Nanoparticles are deposited on electrode surface and used as ion-to-electron transducing coating in ISE. Multi wall carbon nanotubes (MWCNT) have unique structures with excellent electrical and thermal properties. They are known to be inert and highly stable in wide pH range. Besides, being highly hydrophobic, MWCNT can interfere with the formation of water layer between the electrode ion sensing membrane.[40] Moreover, they reduce signal drift which is a known disadvantage of SC-ISEs application. A synergistic effect between these MIP and nanocomposites can help in the specific determination of the desired drugs.

In this study, a novel screen-printed potentiometric sensor was fabricated for determination of PXM either in pharmaceutical formulations or human plasma. Cu(II)-PXM complex was synthesized and employed as neutral carrier for drug sensing. It was compared to traditional ion exchangers used for PXM determination. The sensor was based on MIP for PXM to overcome selectivity challenge. The synthesized MIP was characterized by different techniques including Fourier-transform infrared (FT-IR) spectroscopy, field-emission scanning electron microscope (FE-SEM) and Brunauer–Emmett–Teller (BET) surface area measurements to assess the efficacy of imprinting, removal and rebinding of the PXM templates. MWCNT and graphene nanocomposites (GNC) were then doped on the electrode surface and compared as ion-to electron transducer to reduce water layer and increase signal stability. Finally, the performance characteristics of the proposed sensors were investigated. The Cu-PXM complex based on MIP and MWCNT as a transducer exhibited better performance compared to the proposed fabricated sensors. It was employed for PXM determination in pharmaceutical dosage form and spiked human plasma samples.

2 Experimental

2.1. Chemicals and samples

PXM standard (purity 98.87% ± 0.56) was kindly supplied by Pharco Pharmaceuticals (Egypt). Feldene® dispersible tablets, with labeled amount of 20 mg PXM for each tablet, were manufactured in Pfizer, USA. Carbon screen-printed electrodes (SPE) 3 mm diameter were purchased from CH Instruments, Inc. (USA). High molecular weight polyvinyl chloride (PVC), tridodecyl methyl ammonium chloride, tetradodecyl ammonium bromide, benzethonium chloride, cetylpyridinium chloride, β-cyclodextrin (BCD), calix[6]arene (CX-6), tetrahydrofuran (THF), and multiwalled carbon nanotubes (MWCNT), graphene nanoplatelets (6–8 nm thick × 5 microns wide), methacrylic acid (MAA), dimethylsulfoxide (DMSO), ethylene glycol dimthacrylate (EGDMA), ethanol, methanol, glacial acetic acid and diethyl ether were all purchased from Sigma-Aldrich (Germany). Azobisisobutyronitrile (AIBN), 2-nitrophenyloctyl ether (NPOE) were obtained from Alfa Aesar (Germany). Copper acetate

monohydrate ($Cu(CH_3COO)_2 \cdot H_2O$) was purchased from Loba Chemie (India). Sodium chloride, ammonium chloride, lactose, starch and sodium lauryl sulphate were obtained from El-Nasr Pharmaceutical Chemicals Co (Egypt). Phosphate buffer (pH 8.0 ± 0.2) was prepared using monobasic potassium phosphate solution and then adjusting the pH using 0.2 M NaOH according to the US pharmacopoeia.[41] Human plasma was obtained from Holding Company for Biological Products and Vaccines, VACSERA (Egypt). Double distilled water was used all through the study. All other reagents and chemicals used were of analytical grade.

2.2. Instruments

Potential measurements were carried out using ADWA AD1030 potentiometer (Romania) with Ag/AgCl double-junction reference electrode (Thermo Scientific, USA). pH glass electrode (Jenway, UK) was used for pH adjustment. To assess MIP chemical bonding and identify functional groups, Fourier-transform infrared (FT-IR) spectroscopy was carried out using Shimadzu IRAffinity-1 in addition to field-emission scanning electron microscope (FE-SEM) Quanta 250 FEG model, Fei Company, Oregon-USA). NOVA touch 4LX analyzer (Quantachrome, USA) was used for Brunauer–Emmett–Teller (BET) measurements.

2.3. Procedures

2.3.1. Preparation of Cu-PXM complex. The stoichiometry of Cu(II) binding to PXM was previously reported and determined using mole-ratio method or Job's plot and was found to be 1 : 2 (metal to drug).[42] The Cu-PXM complex has been prepared as described in literature.[43] A hot ethanol solution (60 °C) of $Cu(CH_3COO)_2 \cdot H_2O$ (0.5 mM, 25 mL) was added to hot ethanolic solution (60 °C) of PXM (1 mM, 25 mL). The resulting mixture was magnetically stirred for 30 min under reflux. A yellow coloured complex was formed and precipitated as microcrystalline powder. The complex was then removed by filtration, washed with hot ethanol followed by diethyl ether and left to dry at room temperature.

2.3.2. Preparation of molecular imprinted polymer for PXM. For MIP preparation, non-covalent imprinting method (precipitation polymerization) was employed.[44–46] In a glass stoppered flask 1.0 mmol of PXM was dissolved in 40.0 mL DMSO as a porogenic solvent. For *in situ* precipitation polymerization, 4.0 mmol of MAA as a functional monomer was added followed by sonication for 10.0 min. Then, 25.0 mmol of the cross-linker EGDMA and 1.0 mmol of the initiator AIBN were added. Finally, the flask was purged with nitrogen for almost 10.0 min then placed for 24.0 h in a thermostatic water bath adjusted at 60.0 °C to start polymerization. The formed white precipitate was washed with ethanol and then filtered by decantation to remove excess unreacted reagents. A batch-mode Soxhlet extraction was used for PXM template extraction in which MIP particles were treated with methanol and glacial acetic acid mixture (9 : 1, by volume). Complete extraction was confirmed using UV/vis spectrophotometric measurements by giving no absorbance of PXM in the extracted solutions. The MIP particles were finally washed many times with double distilled water till neutral pH and then dried at 60.0 °C for 2 h. Non-imprinted polymer (NIP) was synthesized using same procedure without adding the PXM template. The morphology of the prepared PXM MIP and NIP were characterized by Fourier-transform infrared (FT-IR) spectroscopy, field-emission surface electron microscope (FE-SEM), Brunauer–Emmett–Teller (BET) surface area measurements.

2.3.3. Fabrication of ISE sensors. For liquid contact (LC) membranes; five sensing mixtures were prepared in which 190.0 mg PVC were mixed with 0.4 mL NOPE and 10.0 mg of either tridodecyl methyl ammonium chloride (sensor I), or tetradodecyl ammonium bromide (sensor II), or benzethonium chloride (sensor III), or cetylpyridinium chloride (sensor IV) or the prepared Cu-PXM complex (sensor V) in a glass test tube using 6.0 mL THF. The five prepared solutions were then poured in a small Petri dish of 5.0 cm diameter and then the solvent was left to evaporate overnight at room temperature, resulting in a master membrane with a thickness of almost 0.1 mm.

For ionophore-doped membranes; the Cu-PXM complex membrane (sensor V) was prepared as mentioned before but with addition of 10.0 mg of the sensing polymers MIP and NIP of PXM (Cu-PXM/MIP, Cu-PXM/NIP). For evaluation of the ionophores' selectivity, two different membranes were prepared in which the sensing polymers (MIP and NIP) were replaced with BCD in one and CX-6 in the other. The Cu-PXM complex and the ionophores, BCD and CX-6, were doped in 1 : 2 molar ratio in the membranes.

For solid contact membrane; MWCNT were prepared according to a previously reported method[47] in which 15 mg MWCNT and 0.5 mL NPOE were dissolved in 3 mL THF. The mixture was then sonicated for 20 min to form a uniform suspension. In a 25-mL volumetric flask, a working solution of MWCNT was prepared by accurately transferring 2.5 mL from the stock solution, diluting to the mark by THF and was sonicated for 5.0 min to ensure dispersion. Graphene nanocomposite (GNC) (1% w/v) was also prepared using solution dispersion method.[48] 10.0 mg graphene nanoplatelets powder were dispersed into 1.0 mL xylene by ultrasonication for 5 min. 95.0 mg PVC and 0.20 mL NPOE as a plasticizer were then dissolved into 3.00 mL of THF. The graphene dispersion was mixed with THF solution and sonicated for 10 min to obtain a uniform suspension.

For screen-printed sensor (without transducer, sensor VI). 10.0 μL of the Cu-PXM/MIP membrane before dryness was drop-casted on a carbon SPE and left to evaporate overnight at room temperature.

For MWCNT screen printed sensor (sensor VII). 10.0 μL of the prepared MWCNT dispersion was drop-casted on a carbon SPE and allowed to evaporate overnight at room temperature. Then, 10.0 μL of the Cu-PXM/MIP membrane before drying was applied to a carbon SPE and left to evaporate overnight at room temperature.

For GNC screen printed sensor (sensor VIII). 10.0 μL of the prepared GNC dispersion was drop-casted on a carbon SPE and allowed to evaporate overnight at room temperature. Then, 10.0

μL of the Cu-PXM/MIP membrane before drying was applied to a carbon SPE and left to evaporate overnight at room temperature.

2.3.4. Liquid contact ion selective electrode assembly. From the master membrane of the five prepared sensors, about 8 mm in diameter disk was cut by using a cork borer and then fixed by THF to a transposable PVC tip. Equal volumes of 1.0×10^{-4} M PXM and 1.0×10^{-4} M NaCl (prepared in 50 mM phosphate buffer, pH 8.0) were mixed and used as an internal reference solution. An Ag/AgCl wire was immersed in the internal reference solution and used as an internal reference electrode. The sensor was soaked in a 1.0×10^{-4} M PXM stock standard solution for 24 h for conditioning and it was then stored in the same solution when not in use. For the ionophore-doped membranes, same procedure was used.

2.3.5. Screen-printed ion selective electrodes (SPEs) assembly. The three fabricated SPE sensors were soaked in 1.0×10^{-4} M PXM stock standard solution for 24 h. For conditioning and were then stored in the same solution when not in use.

2.4. Potentiometric measurements

Stock standard solution of PXM (1.0×10^{-3} M) was prepared in 50.0 mM phosphate buffer pH 8.0 in a 100-mL volumetric flask. Working solutions of varying concentrations (1.0×10^{-7} to 1.0×10^{-4} M) were freshly prepared into a series of 25-mL volumetric flasks. Different volumes were accurately transferred from PXM stock solution (1.0×10^{-3} M) and then completed till the mark using phosphate buffer pH 8.0 as a solvent. Potentiometric measurements were carried out at 25 °C using each of the prepared conditioned sensors. Each sensor was separately conjugated with double junction Ag/AgCl reference electrode then calibrated by immersing it in PXM working standard solutions (1.0×10^{-7} to 1.0×10^{-3}) and allowing it to equilibrate while stirring using a magnetic stirrer till achieving a constant reading of the potentiometer. The electromotive forces (emf) were recorded within ±1 mV. After each measurement, the sensors were washed with the phosphate buffer. The recorded electrode potentials obtained by the proposed sensors were plotted *versus* −log molar concentrations of PXM to construct the calibration curve. Regression equations were estimated from the linear part of the calibration plots. The detection limit of the sensors was estimated from the intersection between the two linear extrapolated arms of background potential and the constructed calibration curve. The performance characteristics of the proposed electrodes were evaluated according to the IUPAC recommendations.[49]

2.5. Effect of pH on MWCNT/Cu-PXM/MIP screen printed sensor

The effect of pH on the response of MWCNT/Cu-PXM/MIP sensor was studied over a pH range of 2–12 using the 1.0×10^{-4} M and 1.0×10^{-3} M PXM solutions. The potential was recorded at each pH value.

2.6. Sensors potential stability and water layer test

The water layer test was implemented by measuring the response of the three SPEs for 3 h. The first hour in 1.0×10^{-3} M PXM. The second hour in 1.0×10^{-2} M perindopril. While the third hour in 1.0×10^{-3} M PXM again.[50] The signal drift was assessed by recording emf values every 2 min during the first hour.

2.7. Selectivity of MWCNT/Cu-PXM/MIP screen printed sensor

The degree of interference of foreign substances with PXM using MWCNT/Cu-PXM/MIP screen printed sensor was studied using the separate solutions method (SSM).[51] The response of the sensor was recorded in the presence of several additives and inorganic-related compounds. The potentiometric selectivity coefficient (K^{Pot}) was calculated.

2.8. Direct potentiometric determination of PXM

2.8.1. Application in pharmaceutical formulation. The average weight of ten tablets of Feldene® was estimated, then the tablets were finely powdered. An amount equivalent to 3.31 mg of PXM was accurately weighed, transferred into a 100-mL volumetric flask, and diluted using 50 mM phosphate buffer (pH 8.0). The flask was sonicated for 15 min till complete dissolution. The concentration of the solution was claimed to be 1.0×10^{-4} M PXM. The MWCNT/Cu-PXM/MIP screen printed sensor in conjunction with the double-junction Ag/AgCl reference electrode was immersed in the prepared solution. The resulting potentials were recorded, and the corresponding concentrations were determined using the sensor's regression equation.

2.8.2. Application in spiked human plasma. One mL of PXM-free human plasma and aliquots of PXM working standard solutions (1.0×10^{-7} to 1.0×10^{-3} M) were added into a series of 10-mL volumetric flasks. The volumes were completed to the mark with phosphate buffer pH 8.0 to give final concentrations of 9.7×10^{-7} M, 2.7×10^{-5} M, 1.5×10^{-5} M, and 2.5×10^{-3} M. The MWCNT/Cu-PXM/MIP screen printed sensor in conjunction with the double-junction Ag/AgCl reference electrode was immersed in the prepared solutions without pre-treatment of matrix. The resulting potentials were recorded, and the corresponding concentrations were determined using the sensor's regression equation.

3 Results and discussion

Screen-printing electrodes are promising potentiometric approaches that have various advantages over traditional analytical methods. They provides non-destructive, rapid, portable, and eco-friendly analytical procedures for detecting analytes in different matrices with no or less sample preparation.[52] To present an alternative efficient method to chromatographic techniques in quantifying PXM in real human plasma samples, the designed sensors should achieve LOQ lower than Cmax of PXM in plasma. This is crucial to detect not only the peak concentration of the drug but also measure the decline in concentration as the drug is metabolized and eliminated from the body also to monitor drug levels over time to see when the drug concentration falls below therapeutic levels, which is

important for therapeutic drug monitoring to ensure proper dosing and effectiveness. This ability is essential for real-time drug monitoring, pharmacokinetic studies, and therapeutic drug monitoring, providing a more efficient, cost-effective, and real-time alternative to traditional chromatographic method. PXM was found to reach a peak plasma concentration of 1.85 μg mL^{-1} (equivalent to 5.58×10^{-6} M) after 1 h from administration of 20 mg PXM.[53] In this study, the impact of ion sensing membrane, ionophore, and the transducer on the fabricated sensors' response sensitivity, selectivity and stability were investigated. Optimization of such factors would have a synergic effect on the electrochemical performance of the developed sensor.

3.1. Fabrication of liquid contact ISE sensors

ISE sensors are fabricated using a polymeric PVC matrix, which acts as a consistent support. However, it needs plasticization, so NPOE was incorporated to provide the membrane malleability. PXM is an enolic acid and exhibits a weakly acidic 4-hydroxy proton. The strongest acidic pK_a value of PXM is 4.76, thus it behaves as an anion in a basic medium. The key factor in the fabrication and optimization of ISE is the type of the used ion exchanger membrane. Therefore, a preliminary study was conducted using LC sensors to assess the effect of the anion exchanger type on potentiometric performance. Five LC-ISE were fabricated for PXM determination with an anion exchanger. It offered cationic sites inside the membrane matrix to increase the conductivity and reduce lipophilic cations interference.[54] Upon using the lipophilic ion exchangers, tridodecyl methyl ammonium chloride, tetradodecyl ammonium bromide, benzethonium chloride (hyamine), and cetylpyridinium chloride, a relatively weak Nernstian slope was obtained (Table S1†). The anionic response of these electrodes is based on ion-exchanger property between the analyte (PXM) anion and the counter ion in which they respond to anions in an order of decreasing hydrophobicity, which is known as Hofmeister selectivity series.[55] When charges of membrane carriers and analyte anions are fixed, the Hofmeister selectivity pattern of classical liquid ion-exchange membrane electrodes can be changed by the coordination affinity. This selectivity is known as anti-Hofmeister series.[33,56] Thus, studies on ISEs with anti-Hofmeister selectivity series with electrical active material that can recognize the specific target ion with higher performance is of great interest due to the urgent need for sensitive determination of traces of anionic species in a wide variety of real samples. Owing to the low lipophilicity of some analytes, the design of a selective ligand for its selective recognition has been a challenging issue. Literature reported several electrodes based on organometallic compounds[57] metal ion complexes[58] and different metalloporphyrin derivatives.[34] Cu-PXM complex was synthesized in a molar ratio of 1 : 2 metal to drug (Fig. S1†) and used as a metal carrier for PXM in fabrication of sensor V as PXM was found to be highly selective to copper.[59] The Cu-PXM LC sensor showed slightly higher sensitivity than the other LC sensors with a Nernstian slope 26.95 ± 0.5 per each drug ion. The introduction of ionophores to Cu-PXM LC sensor was then investigated using β-CD and CX-6, but they showed no significant improvement in the sensor's sensitivity. The Nernstian slope was found to be 26.16 ± 0.9 and 25.82 ± 0.5 upon adding β-CD and CX-6, respectively. To improve the sensor's response, MIP which creates highly efficient synthetic molecular receptors was synthesized and incorporated in the Cu-PXM sensing membranes rather than the traditional ionophores.

3.2. Synthesis and characterization of PXM MIP

MIP is considered an effective approach in which any template molecule is introduced in a mixture of monomer and cross-linker dissolved in a solvent result into three-dimensional polymer matrix. After the removal of template from the prepared polymer, the permanent cavities of the initial template are formed and capable to selectively rebind to template molecules.[60] MIPs have become increasingly popular in sensor technologies owing to their high selectivity, sensitivity, and versatility. They are engineered to have a selective recognition site for a specific target analyte, similar to how natural biological receptors function ensuring high specificity for the target analyte. MIPs provide consistent and reproducible sensor's performance, ensuring reliable results. MIP based sensors offer high sensitivity and low detection limits, suitable for detecting trace analytes.[61] Precipitation polymerization method was employed for synthesis of PXM MIP and NIP to be used as molecular ionophores in the ISE membranes. Precipitation polymerization results in formation of regular size and shape polymer particles which offers more binding sites and good dispersion in the ion sensing membrane.[62] The functional monomer was chosen as per the chemical structure of PXM (Fig. S2†) where basic amino group exists. That's why MAA was selected as an acidic functional monomer. The ratio between the template drug PXM and MAA was adjusted to 1 : 4 being the most optimized ratio for MIP synthesis either in electro-analysis as previously reported in literature.[63] The synthesized PXM MIP was characterized by different techniques as described below.

3.2.1. Field-emission scanning electronic microscope (FE-SEM). The synthesized PXM MIP and its corresponding NIP, were characterized by FE-SEM to investigate their surface morphology as shown in Fig. 1. The figure showed that PXM MIP (Fig. 1a) exhibits more porous and rough structure in comparison with the plain surface of its corresponding NIP (Fig. 1b). This porous pattern is due to the pores and small cavities obtained after PXM templates removal.

3.2.2. Fourier-transform infrared (FT-IR) spectroscopy. The FT-IR spectra of PXM along with its corresponding leached MIP and NIP were recorded over a wavelength range of 4000–500 cm^{-1}.[64] The IR spectrum of PXM was characterized by the presence of two sharp bands, 3336 cm^{-1} due to pyridin-2-yl-amino and hydroxyl stretching and 1631 cm^{-1} due to C=O amide stretching. Aromatic C=C stretching vibrations were also observed at 1575–1560 cm^{-1} (Fig. S3a†). On the other hand, IR spectrum of leached MIP (Fig. S3b†) and NIP (Fig. S3c†) did not have any characteristic IR bands of PXM template drug which gives a strong proof to the removal of PXM template. While keeping the characteristic polymer bands, aliphatic C=C

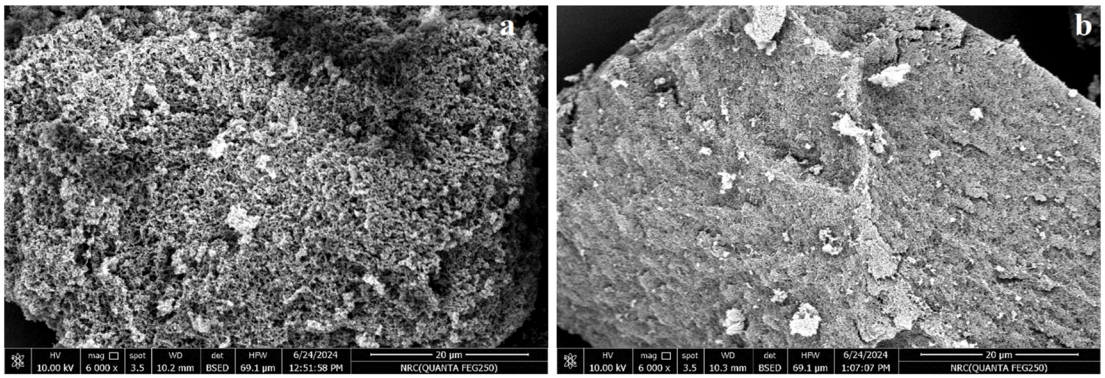

Fig. 1 SEM images for the synthesized (a) PXM MIP and (b) its corresponding NIP.

bands of MAA and EGDMA at 1732 cm^{-1}. The relatively similar IR bands of the leached MIP and NIP suggested that they both have similar backbone structures.

3.2.3. Brunauer–Emmett–Teller (BET) surface area analysis. The porosity extent of the synthesized PXM MIP and its corresponding NIP were estimated from BET measurements. There is a significant influence of polymers' surface area and pore size on their imprinting functionality. Measurements were performed at liquid nitrogen temperature of −196 °C where adsorption/desorption isotherms were recorded as shown in Fig. S4.† These isotherms were used to calculate the specific surface area of polymers using BET equation.[65] Pore volume and diameter were also calculated using the non-local density functional theory (NLDFT).[66] The results are summarized in Table S2.† Results showed larger surface area and average pore volume of MIP compared to their corresponding NIP. This reflected MIP higher porosity than NIP due to the formed imprinted drug cavities during polymerization process. NLDFT results also showed that the diameter of polymers pores was less than 2 nm which is classified as micro pore according to the IUPAC definition.[67]

3.3. Fabrication of screen-printed electrodes (SPEs)

Nanoparticles have been employed in fabrication and optimization of stable solid contact ion selective electrodes for several applications.[68] Various methods were previously reported in literature to employ MWCNT[69,70] and GNC[71,72] as a transducer layer in SPEs to increase potential stability and minimize potential drift. The obstacle of water layer formation in SPE was overcomed by comparing the doping effect of MWCNT and GNC on the sensors' signal stability. The formation of a water layer on the surface of SPEs can affect the stability, sensitivity, and accuracy of the measurements, interfering with the electrochemical reactions, or disrupting the electrode's performance. Transducer materials such as carbon-based nanomaterials can impart hydrophobic properties to the electrode surface. This can help to repel water molecules, preventing the accumulation of a water layer on the electrode surface, making it easier for the

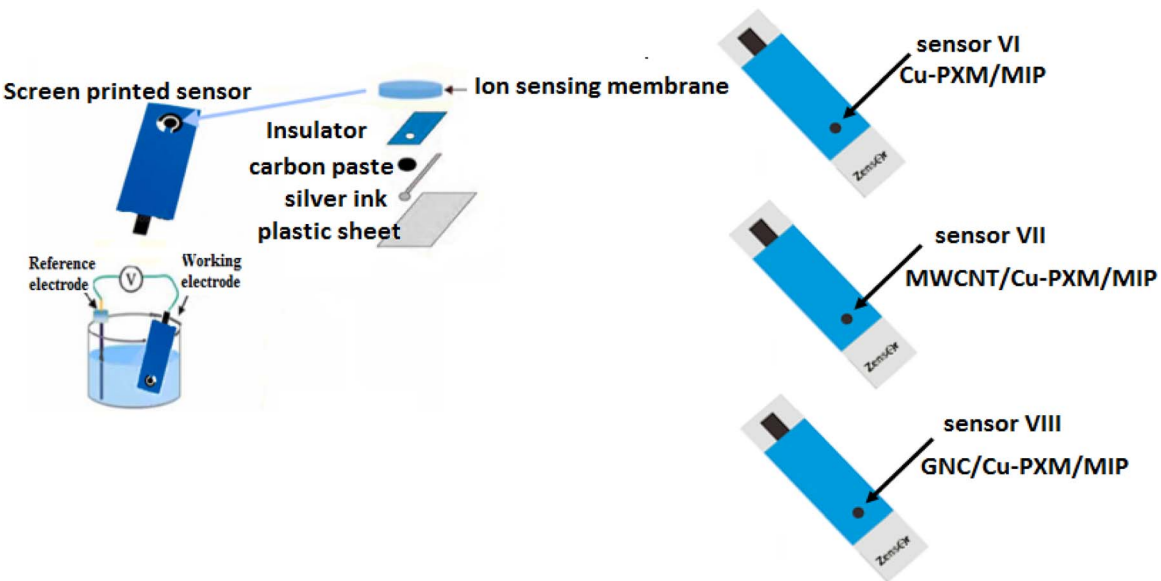

Fig. 2 Schematic representation of screen-printed electrodes (VI–VIII).

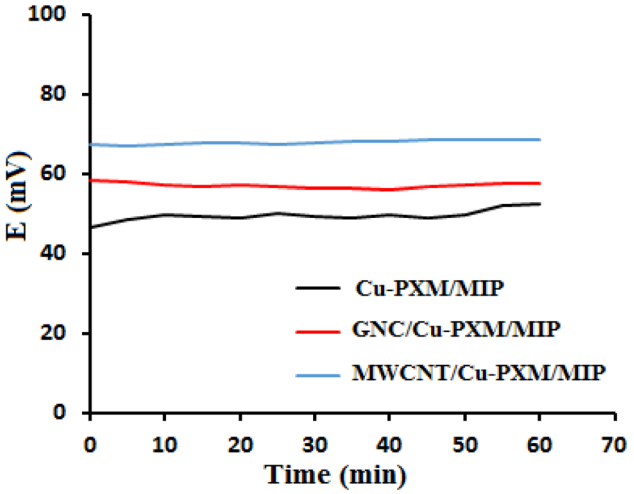

Fig. 3 Signal drift for the three proposed SPEs. Measurements were recorded in 1.0 × 10^{-3} M PXM.

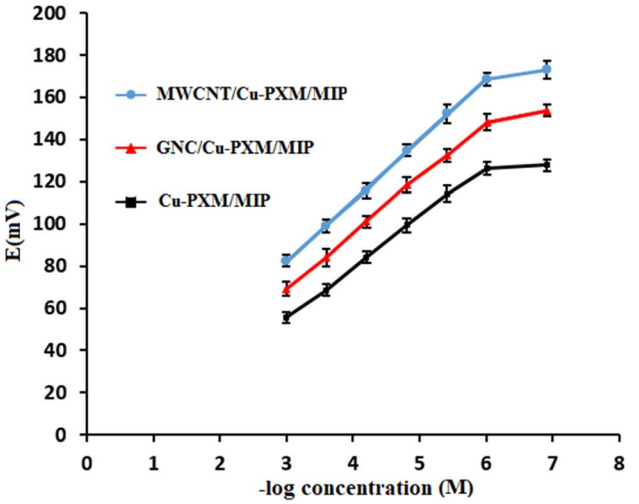

Fig. 4 Potential profile *versus* log concentrations of PXM (1.0 × 10^{-7}–1.0 × 10^{-3} M) obtained with MWCNT/Cu-PXM/MIP, GNC/Cu-PXM/MIP and Cu-PXM/MIP sensors.

sensor to maintain stable electrochemical measurements.[73] Two SPE sensors were fabricated using MWCNT (sensor VII) and GNC (sensor VIII) in which 10 μL of each was drop-casted on SPE modified with MIP based Cu-PXM ion sensing membrane (Fig. 2). Both MWCNT and GNC sensors showed improvement in stability and minimal signal drifting of approximately 0.8 mV h^{-1} and 1.5 mV h^{-1} respectively when compared to the Cu-PXM SPE (sensor VI) which showed signal drifting of about 9.5 mV h^{-1} (Fig. 3). These results confirmed that adding nanoparticles to SPEs significantly improves both electrode stability and signal drifting.

3.4. Sensor's calibration and response time

The IUPAC guidelines were followed to assess the performance characteristics of MWCNT/Cu-PXM/MIP, GNC/Cu-PXM/MIP and Cu-PXM/MIP sensors. The response properties of the proposed SPE sensors were measured over a six-week time frame and the results are shown in Table 1. Calibration curves were plotted for the electrode potential from the proposed SPE sensors *versus* the −log molar concentrations of PXM as shown in Fig. 4. The slope was calculated using the calibration graph's linear portion as shown in Table 1. Better Nernstian slope of 28.97 mV/decade was achieved for MWCNT/Cu-PXM/MIP sensor with respective LOD of 5.2 × 10^{-7} M. This improvement in the sensor's performance may be attributed to synergistic effect upon implementing MWCNT and MIP of PXM. Accuracy, repeatability and intermediate precision of the sensors were also estimated with satisfactory mean percentage recoveries and low relative standard deviations. The MWCNT/Cu-PXM/MIP sensor's stability was evaluated over a six-week period, demonstrating consistent accuracy and reliability. Additionally, repeatability was examined by testing three replicates of the sensor (A, B and C), as illustrated in Fig. 5.

3.5. Sensors potential stability and water layer test

Upon carrying measurements in 1.0 × 10^{-2} M solution of the structurally relative compound, perindopril, increase in the

Table 1 Response characteristics of the proposed SPE sensors for PXM determination

Parameter	Cu-PXM/MIP	GNC/Cu-PXM/MIP	MWCNT/Cu-PXM/MIP
Slope (mV per decade)	25.04	26.51	28.97
Intercept (mV)	−16.97	−10.53	−5.01
Correlation coefficient (r)	0.9993	0.9995	0.9997
Concentration range (M)	1.0 × 10^{-6}–1.0 × 10^{-3}	9.7 × 10^{-7}–1.0 × 10^{-3}	9.7 × 10^{-7}–1.0 × 10^{-3}
Working pH range	7–9	7–9	7–9
Response time (s)	15	10	10
Stability (weeks)	6	6	6
Accuracy ± SD[a]	101.53 ± 1.31	101.62 ± 0.69	101.66 ± 0.81
Repeatability RSD[b]	1.12	0.85	0.74
Intermediate precision RSD[c]	1.44	0.97	1.39
LOD (M)[d]	8.3 × 10^{-7}	6.4 × 10^{-7}	5.2 × 10^{-7}

[a] Average of three determinations ($n = 9$). [b] The intraday precision ($n = 9$), average of three concentrations repeated three times within the same day. [c] The inter-day precision ($n = 9$), average of three concentrations repeated three times on three consecutive days. [d] Limit of detection was measured by interception of the extrapolated arms of the non-responsive and the Nernstian segments of the calibration plot.

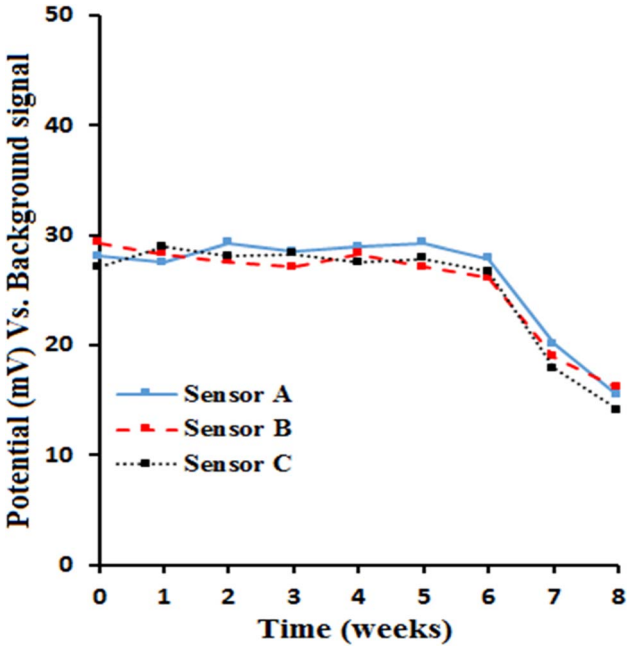

Fig. 5 Stability of MWCNT/Cu-PXM/MIP using 3 replicate sensors (A–C). Measurements were recorded in 1.0×10^{-3} M PXM.

potential was observed. The interferent ion has the same ionic behavior as PXM at the same working pH. This increment in potential is due to the substitution of PXM in the water film formed between the sensing membrane the MWCNT layer and the GNC layer of the sensors by perindopril. The final replacement of the test solution (1.0×10^{-2} M perindopril) by the original 1.0×10^{-3} M PXM solution exhibited lower drift MWCNT/Cu-PXM/MIP sensor compared to GNC/Cu-PXM/MIP (Fig. 6). Whereas Cu-PXM/MIP sensor lacks the hydrophobic

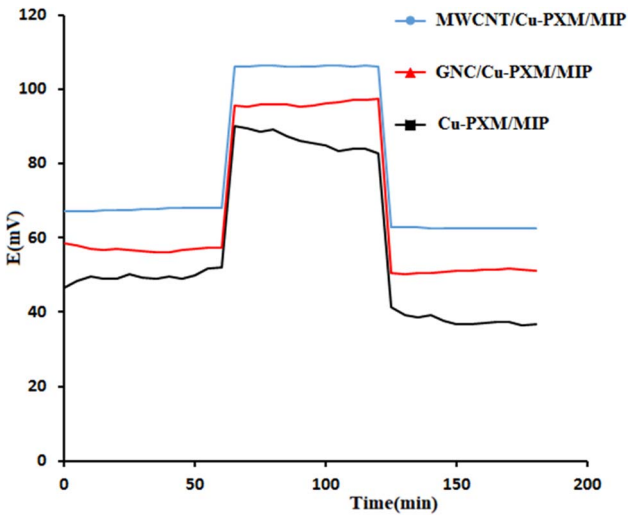

Fig. 6 Water layer test for MWCNT/Cu-PXM/MIP, GNC/Cu-PXM/MIP and Cu-PXM/MIP sensors. Measurements were recorded in 1.0×10^{-3} M PXM then 1.0×10^{-2} M perindopril and finally 1.0×10^{-3} M PXM.

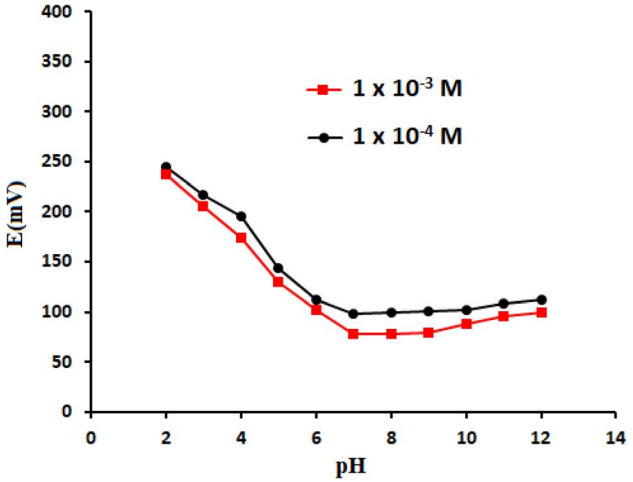

Fig. 7 Effect of pH on the response of MWCNT/Cu-PXM/MIP using the 1.0×10^{-4} M and 1.0×10^{-3} M PXM solutions [working pH range: 7–9].

character of MWCNT and GNC layer. It is clearly demonstrated that MWCNT showed comparable results with GNC. Thus, MWCNT offered the required hydrophobicity for the water layer test. Accordingly, MWCNT/Cu-PXM/MIP sensor was employed for all the measurements determining PXM in Feldene® tablets and spiked human plasma.

3.6. Effect of pH on MWCNT/Cu-PXM/MIP screen printed sensor

A pH study was performed by recording the potential signal of 1.0×10^{-4} M and 1.0×10^{-3} M PXM solution over pH range of 2.0–12.0 (Fig. 7). The pH of the working solutions is such a critical factor to achieve complete drug ionization. A relatively constant potential was obtained within pH range of 7.0–9.0. Higher or lower pH values showed unstable potential possibly due to reduction in the aqueous solubility of PXM and predominance of their molecular form over anionic ones. The strongest acidic and basic pKa of PXM are 4.76 and 3.79 respectively, thus it is highly ionized in the pH range of 7.0–9.0 which increases its solubility. Therefore, a pH value of 8.0 was used to guarantee complete ionization of PXM for its detection.

3.7. Selectivity of MWCNT/Cu-PXM/MIP screen printed sensor

Separate solution method (SSM) was used to detect selectivity of the MWCNT/Cu-PXM/MIP screen printed sensor in presence of some interfering substances.[74] The selectivity of the sensor was measured in the presence of tablet excipients and some of the inorganic compounds that might be present in pharmaceutical dosage forms or in biological fluids. The following equation was used to calculate the potentiometric selectivity coefficient: $\log(K^{\mathrm{Pot}}) = (E_{\mathrm{PXM}} - E_{\mathrm{I}}/S)$, where K^{Pot} is the potentiometric selectivity coefficient, E_{I} is the potential measured in a 1.0×10^{-3} M solution of the interferent ion, E_{PXM} is the potential

Table 2 Potentiometric selectivity coefficients of MWCNT/Cu-PXM/MIP using separate solution method (SSM)

Interfering compound (1.0×10^{-3} M)	K^{pota}
Lactose	0.031
Starch	0.044
NH_4Cl	0.069
Sodium lauryl sulphate	0.027
NaCl	0.086
Meloxicam	0.011

[a] Average of three determinations.

Table 3 Determination of PXM by MWCNT/Cu-PXM/MIP in spiked human plasma

Spiked human plasma	Recovery[a] (%)	RSD (%)
2.5×10^{-3} M	101.37	0.95
1.5×10^{-5} M	100.62	1.31
2.7×10^{-5} M	98.47	1.65
9.7×10^{-7} M	99.17	1.25

[a] Average of three determinations.

measured in a 1.0×10^{-3} M PXM solution, and S is the slope of the calibration curve. The calculated selectivity coefficients revealed that MWCNT/Cu-PXM/MIP exhibited high selectivity towards PXM and no significant interference from other species was observed (Table 2). In addition, a mixed solution containing final concentration of 1.0×10^{-3} M of same interferants (lactose, starch, NH_4Cl, Sodium lauryl sulphate, NaCl, Meloxicam) was measured. A K^{pot} value of 0.092 was obtained indicating minimum interference compared to PXM signal. This would offer an insight into ionic interactions and matrix effects that may occur in complex real samples, thereby providing a reliable assessment of the sensor's performance.

3.8. Direct potentiometric determination of PXM

3.8.1. Application in pharmaceutical formulation. MWCNT/Cu-PXM/MIP was employed to determine PXM concentration in Feldene® tablets. The percentage recovery estimated from average of three determinations was $101.3 \pm 1.15\%$ with good precision. This indicated the selectivity of the proposed sensor towards PXM in pharmaceutical dosage forms regardless of interfering ions and excipients in the formulation.

3.8.2. Application in spiked human plasma. PXM was successfully determined in real samples of spiked human plasma using MWCNT/Cu-PXM/MIP sensor. NSAIDs are widely used to treat long-term inflammatory conditions. The long-term exposure to such class of pharmaceuticals can cause serious upper gastrointestinal adverse effects, particularly bleeding in higher risk patients, such as the elderly and kidney impairment patients which must take adjusted dose.[75] That's why it's crucial to selectively monitor PXM C_{max} in plasma especially for higher risk patients. Upon applying MWCNT/Cu-PXM/MIP sensor in spiked human plasma samples, satisfactory results were achieved without employing matrix pre-treatment procedures. The incorporation of MIP facilitates the detection of PXM despite the presence of any other interferents, whereas the Cu-PXM complex improved the sensitivity of the sensor to lower detection limit. In addition, the screen-printed electrode offered an economical sensing platform. The percentage mean recoveries of PXM were presented in Table 3. These findings were promising for a direct and feasible determination of PXM without interference either from dosage form or plasma proteins and ions.

3.9. Statistical data analysis and comparison with previously reported potentiometric methods

Results obtained using the proposed MWCNT/Cu-PXM/MIP sensor were statistically compared to those obtained by applying previously reported method for determination of PXM in its pharmaceutical preparation.[32] Student's *t*-test and *F*-test were applied and the calculated *t*- and *F*- test values were found to be less than the tabulated ones indicating insignificant difference between the compared methods (Table S3†). Moreover, the results of the proposed sensor were compared to other reported methods for determination of PXM in terms of linearity range, LOD, ISE used, and their application as shown in Table 4. The proposed sensor had the advantage of having wide linear range with lower detection limit for PXM. Besides, the incorporation of highly specific MIP for the target analyte PXM in the developed sensor allowed the specific determination of PXM in spiked human plasma and complex matrices.

Table 4 Overview of previously reported potentiometric methods for PXM determination

Analyte	Linearity range (M)	LOD (M)	Used ISE	Application	Ref.
PXM & Ketroprofen	1.0×10^{-4}–5.0×10^{-2}	3.2×10^{-5}	Liquid contact ISE	Pharmaceutical dosage form	29
PXM	1.0×10^{-6}–1.0×10^{-2}	7.0×10^{-7}	Solid contact ISE (carbon paste electrode)	Pharmaceutical dosage form	31
PXM & other different oxicams	1.0×10^{-7}–1×10^{-2}	6.0×10^{-7}	Solid contact ISE	Pharmaceutical dosage form Biological fluids	32
PXM	9.7×10^{-7} –1.0×10^{-3}	5.2×10^{-7}	Screen printed ISE	Pharmaceutical dosage form Spiked human plasma	Present work

4 Conclusion

This study introduced a novel potentiometric approach for the determination of PXM. Selective and sensitive SPE was fabricated for the determination of PXM in pharmaceutical dosage form and spiked human plasma. A metal carrier based on Cu-PXM complex was employed as sensitive sensing membrane for detection of PXM. The high recognition capability of MIP based sensor was compared to the effect of ionophores on the selectivity and stability of the proposed sensors. Different characterization techniques including FE-SEM, FT-IR, and BET measurements were employed to assess the efficacy of imprinting, removal and rebinding of the PXM templates in the synthesized MIP. Moreover, the formation of water layer was controlled successfully by adding either MWCNT or GNC as ion-to-electron transducer between the sensing membrane and the electrode surface. The membrane optimization achieved more sensitive determination and lower detection limit in determination of PXM upon using MIP based Cu-PXM complex in combination to MWCNT as a transducer. The proposed SPE sensor offered many advantages, in terms of sensitivity, selectivity, stability, and durability. This enabled their application in spiked human plasma samples where peak concentration of PXM requires more sensitive and selective sensors. Generally, the proposed potentiometric platform offered simplicity in design and a lower detection limit as well as being rapid and economic.

Data availability

The authors confirm that the data supporting the findings of this study are available within the article and its ESI.†

Author contributions

Veronia S. Nazim: methodology, investigation, formal analysis, visualization, writing – original draft. Ghada M. El-Sayed: supervision, validation, resources, writing – review and editing. Sawsan M. Amer: conceptualization, project administration, supervision. Ahmed H. Nadim: methodology, investigation, data curation, formal analysis, validation, resources, writing – review and editing.

Conflicts of interest

The authors declare that they have no known competing financial interests or personal relationships that could have appeared to influence the work reported in this paper.

References

1 A. J. Bard, L. R. Faulkner and H. S. White, *Electrochemical Methods: Fundamentals and Applications*, John Wiley & Sons, 2022.
2 S. S. Nielsen, in *Nielsen's Food Analysis Laboratory Manual*, Springer, 2024, pp. 167–175.
3 A. Ruiz-Gonzalez, *Electrochem*, 2024, **5**, 178–212.
4 M. M. Mostafa, G. A. Sedik, E. S. Elzanfaly and A. H. Nadim, *Anal. Biochem.*, 2023, **683**, 115367.
5 L. Gao, Y. Tian, W. Gao and G. Xu, *Sensors*, 2024, **24**, 4289.
6 Y. H. Cheong, L. Ge and G. Lisak, *Anal. Chim. Acta*, 2021, **1162**, 338304.
7 R. Sharma, M. Geranpayehvaghei, F. Ejeian, A. Razmjou and M. Asadnia, *Talanta*, 2021, **235**, 122815.
8 M. M. Antonisse and D. N. Reinhoudt, *Electroanalysis*, 1999, **11**, 1035–1048.
9 N. W. Nashat, A. M. Mahmoud and A. H. Nadim, *Microchem. J.*, 2025, **208**, 112582.
10 Y. Zhang, J. Zhou, T. Yang, X. Li, Y. Zhang, Z. Huang, G. J. Mattos, N. Y. Tiuftiakov, Y. Wu and J. Gao, *ACS Sens.*, 2024, **9**, 6512–6519.
11 R. Brennan, M. Wazaify, H. Shawabkeh, I. Boardley, J. McVeigh and M. C. Van Hout, *Drug Safety*, 2021, **44**, 917–928.
12 D. Vega-Morales, I. R. M. Pérez-Luna, V. A. Aguirre-García and B. R. Vázquez-Fuentes, *Reumatol. Clin.*, 2021, **17**, 499–503.
13 C. Varas-Lorenzo, N. Riera-Guardia, B. Calingaert, J. Castellsague, A. Pariente, L. Scotti, M. Sturkenboom and S. Perez-Gutthann, *Pharmacoepidemiol. Drug Saf.*, 2011, **20**, 1225–1236.
14 Y. Y. Hnepa, I. V. Chopey, K. I. Chubirko and A. M. Bratasyuk, *Wiad. Lek.*, 2021, **74**, 1011–1018.
15 S. Cox, J. Hayes, J. Yarbrough, T. Veiga-Parga and C. Greenacre, *Chromatogr. Res. Int.*, 2014, **2014**, 521697.
16 G. Dragomiroiu, A. Cimpoiesu, O. Ginghina, C. Baloescu, M. Barca, D. E. Popa, A.-M. Ciobanu and V. Anuta, *Farmacia*, 2015, **63**, 123–131.
17 S. Ivanova, V. Todorova, S. Dyankov and K. Ivanov, *Processes*, 2022, **10**, 394.
18 A. Alsaqqa, J. A. Hasian and A. M. Al-Laham, *Baghdad Sci. J.*, 2023, **20**, 0681.
19 R. M. Mahmood, S. A. Darweesh, N. A. Alassaf and R. S. Al-Khalisy, *Methods & Objects of Chemical Analysis/Metody & Obekty Himičeskogo Analiza*, 2024, p. 19.
20 R. I. Abed and H. Hadi, *Bull. Chem. Soc. Ethiop.*, 2020, **34**, 13–23.
21 R. M. Mahmood, S. A. Darweesh, N. A. Alassaf and R. S. Al-Khalisy, *Methods Objects Chem. Anal.*, 2024, **19**, 101–110.
22 G. Z. D. M. G. de Oliveira, F. W. L. Silva, C. S. C. Lopes, B. F. Braz, R. E. Santelli and F. H. Cincotto, *Ionics*, 2024, **30**, 2793–2806.
23 I. Y. L. d. Macêdo, M. F. Alecrim, J. R. Oliveira, I. M. S. Torres, D. V. Thomaz and E. d. S. Gil, *Braz. J. Pharm. Sci.*, 2020, **56**, e17344.
24 M. Sadeghi, M. Shabani-Nooshabadi and H. Ansarinejad, *Environ. Res.*, 2023, **216**, 114633.
25 X. A. Vu Ho, M. U. Dao, T. H. Le, T. H. Chuong Nguyen, M. T. Nguyen Dinh, Q. M. Nguyen, T. M. Tran, T. T. Huyen Nguyen, T.-T. Ho and H. P. Nguyen, *Ind. Eng. Chem. Res.*, 2023, **62**, 4778–4791.
26 O. Özbek and C. Berkel, *Sens. Int.*, 2022, **3**, 100189.
27 X. Gong, K. Huang, Y.-H. Wu and X.-S. Zhang, *Sens. Actuators, A*, 2022, **345**, 113821.

28 A. Hayat and J. L. Marty, *Sensors*, 2014, **14**, 10432–10453.
29 Z. Kormosh, I. Hunka, Y. Bazel and O. Matviychuk, *Mater. Sci. Eng., C*, 2010, **30**, 997–1002.
30 M. A. El-Ries, G. Mohamed, S. Khalil and M. El-Shall, *hem. Pharm. Bull.*, 2003, **51**, 6–10.
31 E. Khaled, M. S. Kamel, H. N. Hassan, A. A. Haroun, A. M. Youssef and H. Y. Aboul-Enein, *Talanta*, 2012, **97**, 96–102.
32 E. Khaled, M. S. Kamel, H. N. Hassan, S. H. Abd El-Alim and H. Y. Aboul-Enein, *RSC Adv.*, 2015, **5**, 12755–12762.
33 B. Patel, A. Kumar and S. K. Menon, *J. Inclusion Phenom. Macrocyclic Chem.*, 2009, **64**, 239–247.
34 D. Gao, J.-Z. Li, R.-Q. Yu and G.-D. Zheng, *Anal. Chem.*, 1994, **66**, 2245–2249.
35 S. Sadeghi, D. Mohammadzadeh and J. S. Imampur, *Anal. Bioanal. Chem.*, 2005, **383**, 261–267.
36 L. Sun, C. Sun and X. Sun, *Electrochim. Acta*, 2016, **220**, 690–698.
37 R. Liang, L. Kou, Z. Chen and W. Qin, *Sens. Actuators, B*, 2013, **188**, 972–977.
38 G. De Middeleer, P. Dubruel and S. De Saeger, *TrAC, Trends Anal. Chem.*, 2016, **76**, 71–85.
39 F. W. Campbell and R. G. Compton, *Anal. Bioanal. Chem.*, 2010, **396**, 241–259.
40 V. Pifferi, G. Cappelletti, C. Di Bari, D. Meroni, F. Spadavecchia and L. Falciola, *Electrochim. Acta*, 2014, **146**, 403–410.
41 U. Pharmacopeia, *The United States Pharmacopeial*, 2024.
42 S. Roy, R. Banerjee and M. Sarkar, *J. Inorg. Biochem.*, 2006, **100**, 1320–1331.
43 G. M. Gehad and E. E.-G. Nadia, *Vib. Spectrosc.*, 2004, **36**, 97–104.
44 A. M. Hassan, K. M. Kelani, M. A. Hegazy and M. A. Tantawy, *Anal. Chim. Acta*, 2023, **1278**, 341707.
45 M. Roushani, Z. Jalilian and A. Nezhadali, *Colloids Surf., B*, 2018, **172**, 594–600.
46 M. Wadie, H. M. Marzouk, M. R. Rezk, E. M. Abdel-Moety and M. A. Tantawy, *Anal. Chim. Acta*, 2022, **1200**, 339599.
47 Y. Liu, Y. Liu, Y. Gao and P. Wang, *Sens. Actuators, B*, 2019, **281**, 705–712.
48 A. M. Mahmoud, M. T. Ragab, N. K. Ramadan, N. A. El-Ragehy and B. A. El-Zeany, *Electroanalysis*, 2020, **32**, 2803–2811.
49 E. Lindner and Y. Umezawa, *Pure Appl. Chem.*, 2008, **80**, 85–104.
50 D. Yuan, A. H. Anthis, M. Ghahraman Afshar, N. Pankratova, M. Cuartero, G. A. Crespo and E. Bakker, *Anal. Chem.*, 2015, **87**, 8640–8645.
51 R. Bereczki, B. Takács, J. Langmaier, M. Neely, R. E. Gyurcsányi, K. Tóth, G. Nagy and E. Lindner, *Anal. Chem.*, 2006, **78**, 942–950.
52 R. Couto, J. Lima and M. Quinaz, *Talanta*, 2016, **146**, 801–814.
53 C. Rasetti-Escargueil and V. Grangé, *Int. J. Pharm.*, 2005, **295**, 129–134.
54 E. Bakker, P. Bühlmann and E. Pretsch, *Chem. Rev.*, 1997, **97**, 3083–3132.
55 S. Sadeghi, A. Gafarzadeh, M. A. Naseri and H. Sharghi, *Sens. Actuators, B*, 2004, **98**, 174–179.
56 G. Ye, Y. Chai, Y. Ruo, L. Zhou, Y. Li and L. Zhang, *Anal. Sci.*, 2007, **23**, 171–176.
57 U. Wuthier, H. V. Pham, R. Zuend, D. Welti, R. J. J. Funck, A. Bezegh, D. Ammann, E. Pretsch and W. Simon, *Anal. Chem.*, 1984, **56**, 535–538.
58 A. Florido, L. G. Bachas, M. Valiente and I. Villaescusa, *Analyst*, 1994, **119**, 2421–2425.
59 S. Sadeghi, D. Mohammadzadeh and J. S. Imampur, *Anal. Bioanal. Chem.*, 2005, **383**, 261–267.
60 M. Roushani, A. Nezhadali, Z. Jalilian and A. Azadbakht, *Mater. Sci. Eng., C*, 2017, **71**, 1106–1114.
61 A. G. Ayankojo, J. Reut and V. Syritski, *Biosensors*, 2024, **14**, 71.
62 S. A. Mohajeri, G. Karimi, J. Aghamohammadian and M. R. Khansari, *J. Appl. Polym. Sci.*, 2011, **121**, 3590–3595.
63 J. Wang, R. Liang and W. Qin, *TrAC, Trends Anal. Chem.*, 2020, **130**, 115980.
64 G. Socrates, *Infrared and Raman Characteristic Group Frequencies: Tables and Charts*, John Wiley & Sons, 2004.
65 S. Brunauer, P. H. Emmett and E. Teller, *J. Am. Chem. Soc.*, 1938, **60**, 309–319.
66 J. P. Olivier, *J. Porous Mater.*, 1995, **2**, 9–17.
67 J. Rouquerol, D. Avnir, C. W. Fairbridge, D. H. Everett, J. Haynes, N. Pernicone, J. D. Ramsay, K. S. W. Sing and K. K. Unger, *Pure Appl. Chem.*, 1994, **66**, 1739–1758.
68 T. O. Falola, *World J. Nano Sci. Eng.*, 2022, **12**, 29–62.
69 S. A. Hassan, N. W. Nashat, M. R. Elghobashy, S. S. Abbas, A. A. Moustafa and A. M. Mahmoud, *Microchem. J.*, 2022, **178**, 107323.
70 S. SM Hassan, A. Galal Eldin, A. E.-G. E. Amr, M. A. Al-Omar, A. H. Kamel and N. M. Khalifa, *Sensors*, 2019, **19**, 3891.
71 N. S. Anuar, W. J. Basirun, M. Shalauddin and S. Akhter, *RSC Adv.*, 2020, **10**, 17336–17344.
72 S. S. El-Mosallamy, K. Ahmed, H. G. Daabees and W. Talaat, *Anal. Bioanal. Chem.*, 2020, **412**, 7505–7514.
73 H. Meskher, T. Ragdi, A. K. Thakur, S. Ha, I. Khelfaoui, R. Sathyamurthy, S. W. Sharshir, A. Pandey, R. Saidur and P. Singh, *Crit. Rev. Anal. Chem.*, 2024, **54**, 2398–2421.
74 A. A. Mouhamed, B. M. Eltanany, N. M. Mostafa, T. A. Elwaie and A. H. Nadim, *RSC Adv.*, 2023, **13**, 23138–23146.
75 F. Richy, C. Scarpignato, A. Lanas and J.-Y. Reginster, *Pharmacol. Res.*, 2009, **60**, 254–263.